# THIRD DREDGE-UP

- $^{12}C$ from He-shell → C/O increasing in the convective envelope and atmosphere.
- if sufficient $^{12}C$ added to atmosphere, C/O > 1 and star becomes a carbon star.

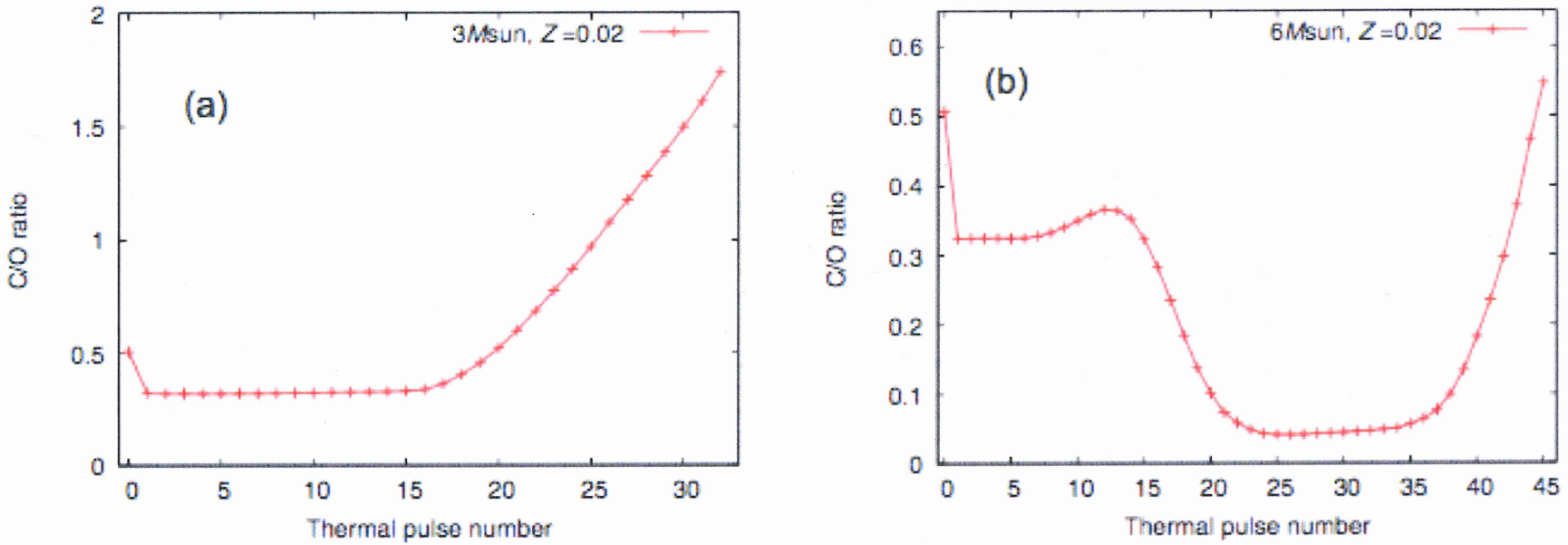


**Figure 21.** The surface C/O ratio as a function of thermal pulse number for (a) a $3\,M_{\odot}$, $Z = 0.02$ model AGB star, and (b) a $6\,M_{\odot}$, $Z = 0.02$ model. The lower mass $3\,M_{\odot}$ model does not experience HBB and becomes C-rich. In contrast, efficient HBB occurs for the $6\,M_{\odot}$ model and the C/O ratio never reaches unity. The C/O ratio is given by number, and the initial abundance is the solar ratio at C/O = 0.506.

0.5 ↓ FDU

C/O ↑ TDU with incr. pulse number

M → MS → S — C star

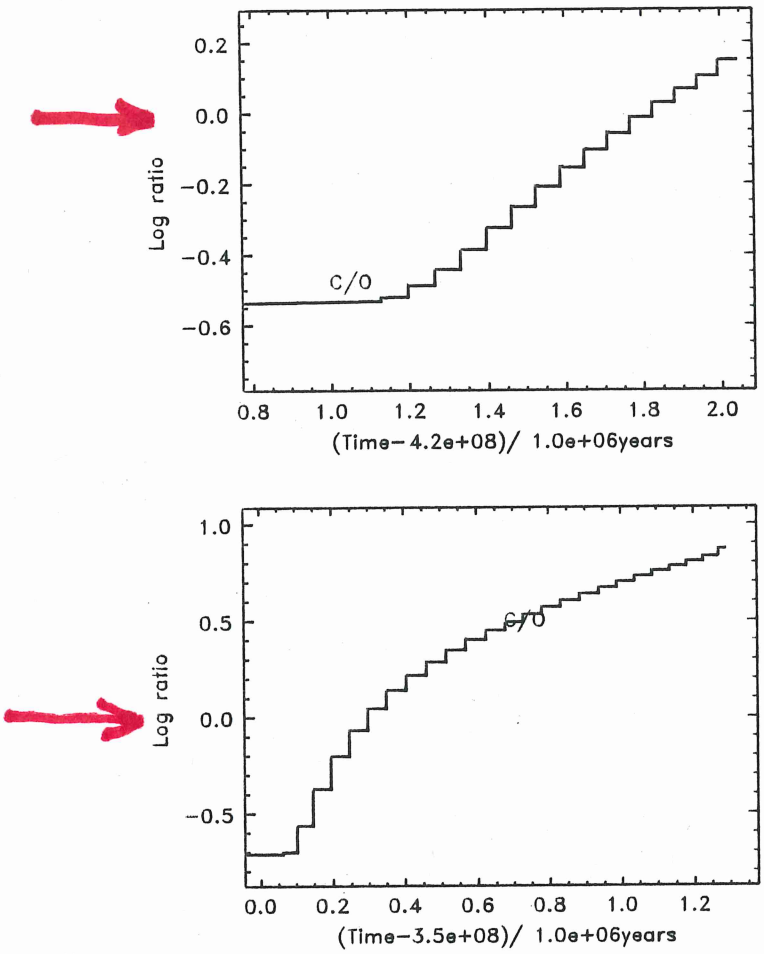


**Fig. 18.** Logarithm of the surface C/O ratio as a function of time during the TP-AGB for two $3M_{\odot}$ models of different metallicity. The top panel shows the C/O ratio from the $Z = 0.02$ model, the lower panel shows results for the lower metallicity $Z = 0.004$ model. Time has been scaled such that the start of the TP-AGB is $t = 0$

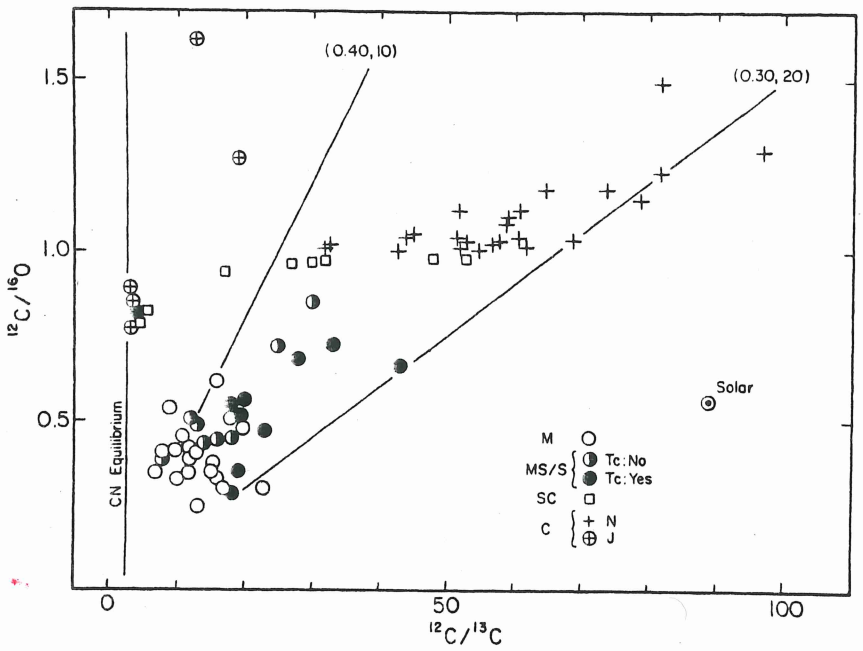


FIG. 9.—$^{12}C/^{16}O$ vs. $^{12}C/^{13}C$ for cool giants. The majority of the giants lie between the solid lines that trace the composition as $^{12}C$ is added to the envelope of a M giant; the lines are labeled with the M giant's initial composition, i.e., ($^{12}C/^{16}O$, $^{12}C/^{13}C$).

# OTHER n-s IN TP-AGBs

## FLUORINE ($^{19}F$)

in He-intershell via

$^{14}N(\alpha,\gamma)^{18}F(e^+,\nu)^{18}O(p,\alpha)^{15}N(\alpha,\gamma)^{19}F$

$^{13}C(\alpha,n)^{16}O$ $\quad$ $^{14}N(n,p)^{14}C$

The fragile element fluorine can be produced inside the He-intershell of AGB stars. Jorissen, Smith & Lambert [130] discovered that the [F/O] abundance correlates with the C/O ratio in AGB stars, and that some N-type carbon stars show surface enrichments a factor of 30 above the solar ratio. The increase in the C/O ratio is clearly a result of the third dredge-up and thermal pulses, hence it was concluded that the carbon and fluorine are produced in the same region in the star and mixed together to the surface. Jorissen et al. [130] examined the many pathways that fluorine, or more precisely the isotope $^{19}$F, could be produced and concluded that the most likely chain is

$$^{14}\mathrm{N}(\alpha,\gamma)^{18}\mathrm{F}(\beta^{+}\nu)^{18}\mathrm{O}(p,\alpha)^{15}\mathrm{N}(\alpha,\gamma)^{19}\mathrm{F}. \quad (4)$$

Fluorine production takes place in the He-intershell, a region that is essentially devoid of protons, and has a very low abundance of $^{13}$C and $^{15}$N. Hence other reactions are required to produce the protons and the $^{15}$N. These other reactions include $^{13}\mathrm{C}(\alpha,n)^{16}\mathrm{O}$ that is required to produce free neutrons; these are subsequently captured by $^{14}\mathrm{N}(n,p)^{14}\mathrm{C}$ to produce free protons. In Figure 22 we show the composition of the He-intershell during and after a thermal pulse. The increase in $^{15}$N and $^{18}$O during the pulse is evident; both of these species are subsequently destroyed and are absent in the lower panel. The resulting $^{19}$F abundance in the He-intershell is more than an order of magnitude greater than in the envelope. Fluorine can also be destroyed via $^{19}\mathrm{F}(\alpha,p)^{22}\mathrm{Ne}$, which is more efficient at temperatures over $\approx 300 \times 10^6$ K [128, 131]. In Figure 23 we show the surface abundance evolution of $^{19}$F for the $3M_{\odot}$, $Z = 0.02$, noting the large increase over the TP-AGB through the repeated action of third dredge-up mixing events. The fluorine abundance increases by about a factor of four.

An example of the many reaction rates that affect the production of fluorine is the alternative proton production reaction $^{18}\mathrm{F}(\alpha,p)^{21}\mathrm{Ne}$ [132]. Including the $^{18}\mathrm{F}(\alpha,p)^{21}\mathrm{Ne}$ reaction reduces the abundance of $^{18}$O because it competes with $^{18}$O production via the $^{18}\mathrm{F}(\beta^{+}\nu)^{18}\mathrm{O}$ decay (the half life of $^{18}$F is 109 minutes). However, the extra amount of protons from $(\alpha,p)$ enhances the $^{18}\mathrm{O}(p,\alpha)^{15}\mathrm{N}$ reaction rate, even though $^{18}$O production has been deprived from the decay. This is shown in Figure 24 for the $3M_{\odot}$, $Z = 0.008$ model, where we also show an example of the effect of reaction rate uncertainties on the nucleosynthesis predictions. We refer the reader to [115], [133], [128], and [132] for more details on the complex production of fluorine in AGB stars.

The cosmic origin of fluorine is not yet completely understood, where Type II SN explosions [134] and stellar winds from Wolf-Rayet stars [135] play a significant role in producing this fragile element alongside AGB stars [136]. Certainly AGB stars and their progeny (e.g., post-AGB stars and planetary nebulae) are the only confirmed site of fluorine production thus far [130, 127, 137, 138], with no clear indication for enhanced F abundances resulting from the $\nu$-process in a region shaped by past SNe [139]. The recent observations of a greatly enhanced fluorine abundance ([F/Fe] = 2.90) in a

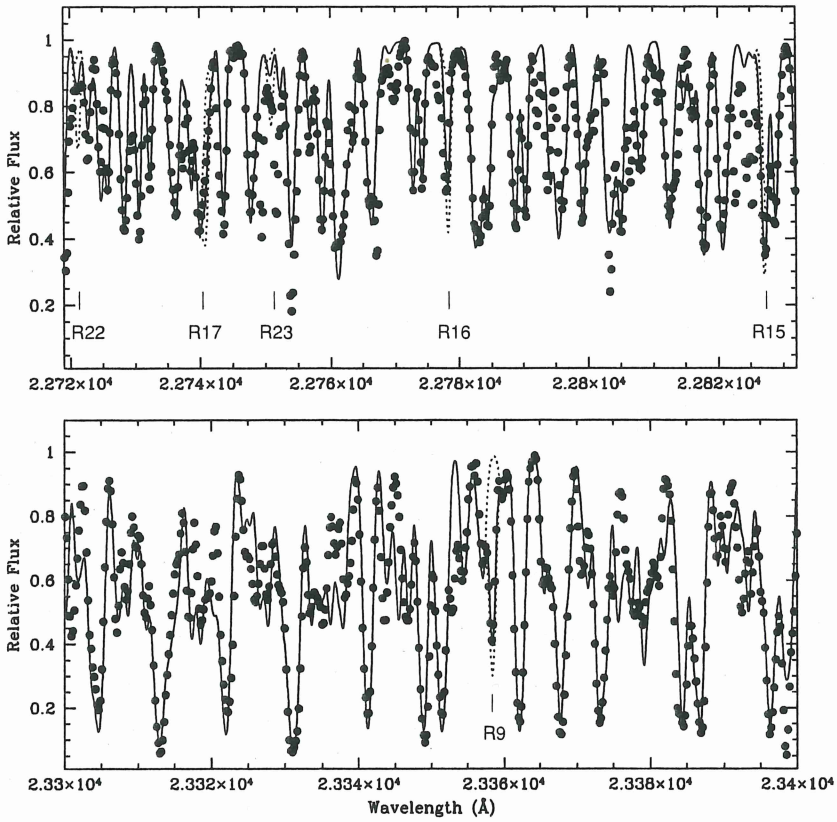


**Figure 1.** Comparison of the observed and synthetic spectra of UU Aur (dots) with an identification of the available HF lines. Dashed lines represent the synthetic spectra calculated with no F and with the abundance value obtained by JSL, respectively. The continuous line is the synthetic spectrum calculated with the abundance given in Table 1, $\log \epsilon(\mathrm{F}) = 4.88$.

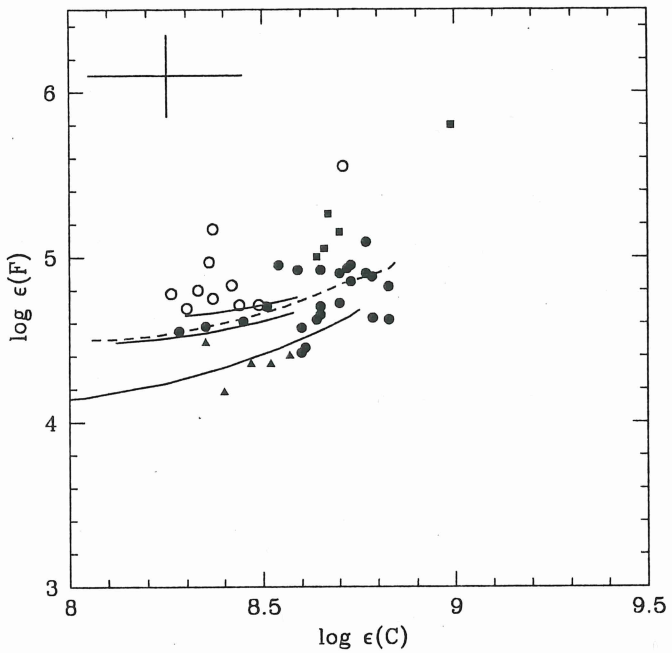


**Figure 2.** Logarithmic abundances of fluorine vs. carbon. Symbols: filled circles, N-stars; triangles, J-type; squares, SC-type; open circles, intrinsic O-rich AGB stars from JSL. Lines are theoretical predictions for a 1.5 $M_{\odot}$, TP-AGB model with metallicities $Z = 0.02$, $Z_{\odot}$, and 0.006 (continuous lines from up to down), and a 2 $M_{\odot}$, $Z = Z_{\odot}$ model (dashed line), respectively.

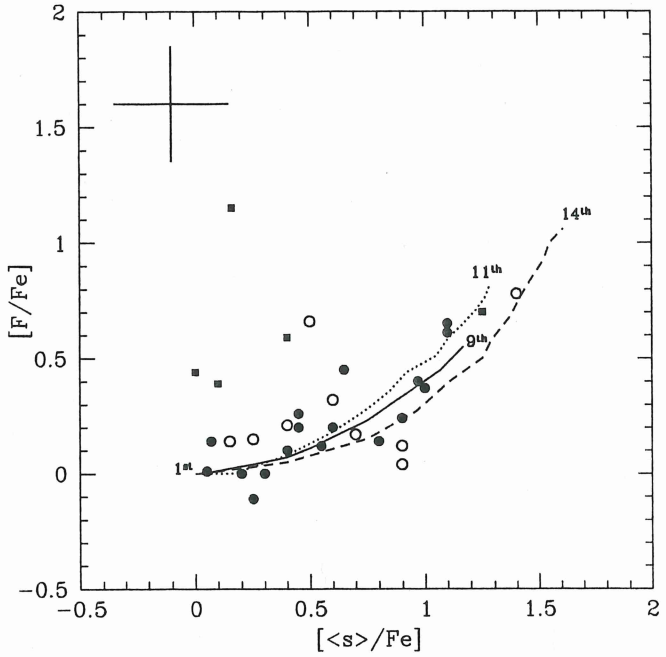


**Figure 3.** Fluorine vs. average *s*-element enhancements in Galactic AGB stars. Symbols as in Figure 2. Lines are theoretical predictions for 1.5, 2, and 3 $M_{\odot}$, $Z = 0.008$ TP-AGB models (solid, dashed, and dotted lines, respectively) from S. Cristallo et al. (2010, in preparation). The number of TPs achieved by each model is also indicated.

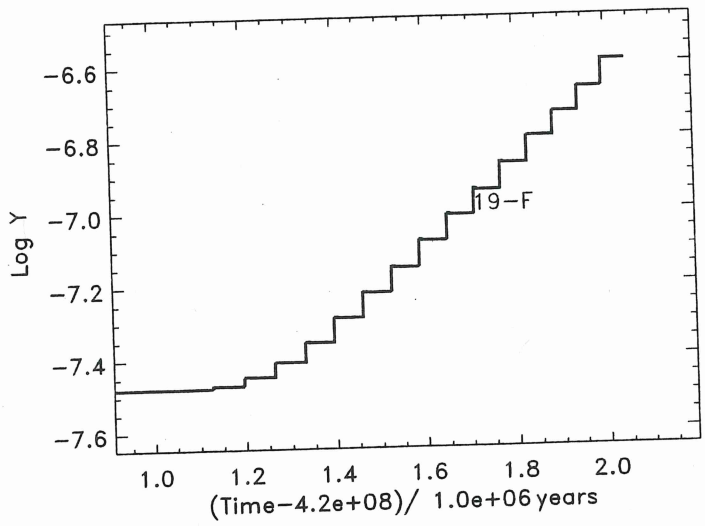


**Fig. 23.** The abundance evolution of $^{19}$F at the surface for the $3M_{\odot}$, $Z = 0.02$ model during the TP-AGB. The $^{19}$F abundance increases by about a factor of 4

carbon-enhanced metal-poor halo star [140] represents further strong motivation to better understand the details of fluorine production in AGB stars [141].

# OTHER n-s IN TP-AGB

## H-BURNING SHELL

- CNO CYCLES : H ⇒ He; C ⇒ N etc
- Ne ↔ Na  Mg ↔ Al  CHAINS

## He-BURNING SHELL

- $^{14}N \Rightarrow {}^{22}Ne$  ← n source

$^{22}Ne(\alpha, n)^{25}Mg$

$(\alpha, \gamma)^{26}Mg$

# HOT BOTTOM CONVECTIVE ENVELOPE

- Li PRODUCTION
  - $^{12}C \rightarrow {}^{14}N$ $^{12}C/^{13}C \sim 3$
- Ne-Na ; Mg-Al CHAINS

### 5.6 Hot bottom burning

In intermediate-mass AGB stars over about $4M_{\odot}$ (depending on $Z$), the base of the convective envelope can dip into the top of the H-burning shell, causing proton-capture nucleosynthesis to occur there (Figure 25). This phenomenon is known as hot bottom burning, and can change the surface composition because the entire envelope is exposed to the hot burning region a few thousand times per interpulse period. For a review of HBB nucleosynthesis see Lattanzio et al. [146]. If the base of the envelope is sufficiently hot, the Ne-Na and Mg-Al chains (Figure 17) may operate alongside the CNO cycle; $^{7}$Li production is also possible via the Cameron-Fowler mechanism [63, 146]. HBB converts the $^{12}$C dredged into the envelope to $^{14}$N, which can prevent the C/O ratio exceeding unity, while keeping the $^{12}$C/$^{13}$C ratio near the equilibrium value $\sim 4$. Frost et al. [147] noted that intermediate-mass AGB stars may become

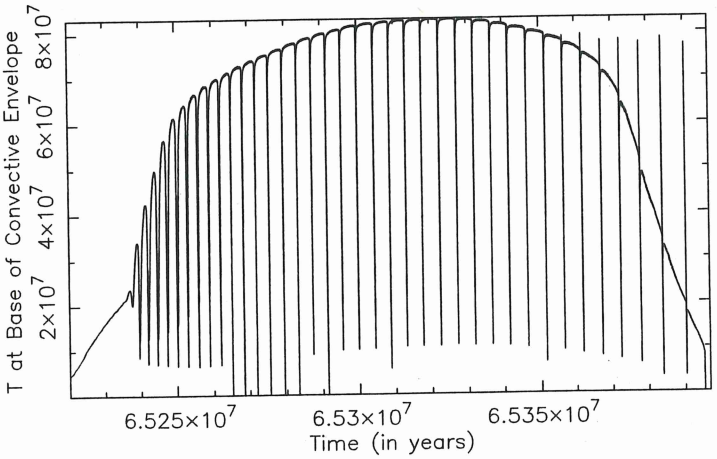


**Fig. 25.** The temperature at the base of the envelope during the TP-AGB phase for a $6M_{\odot}$, $Z = 0.02$ model

luminous, optically obscured carbon stars near the end of the TP-AGB, when mass loss has removed much of the envelope, extinguishing HBB but allowing dredge-up to continue. HBB stars may be important for the production of many elements including nitrogen, lithium, sodium, as well as the magnesium and aluminium isotopes.

### 5.7 The production of lithium by HBB

The observations of Wood, Bessell, & Fox [4] were the first to suggest that the oxygen-rich luminous AGB stars in the Magellanic Clouds are undergoing CNO cycling at the base of the convective envelope, converting the dredged up carbon to nitrogen. The discovery that these stars are also rich in Li [62,63,64] gave further credibility to the idea that HBB was actually occurring in massive AGB stars. The production of $^7$Li is thought to occur via the Cameron-Fowler mechanism [148]: Some $^3$He, created earlier in the evolution (during central H-burning), captures an $\alpha$-particle to create $^7$Be. The $^7$Be can either 1) capture a proton to complete the PP III chain, or 2) capture an electron to produce $^7$Li. Whether the $^7$Be follows path 1) or path 2) depends critically on the temperature of the region. Owing to efficient mixing in the convective envelope (where the convective turnover time is $\approx$ 1 year), some of the $^7$Be is mixed into a cooler region which prevents proton capture. The $^7$Be will undergo electron-capture instead, producing $^7$Li. The $^7$Li is also subject to proton capture and is eventually mixed into the hot temperature region and subsequently destroyed. Once the envelope is depleted in $^3$He, $^7$Li production stops. The Li-rich regime lasts for $\sim$100,000 years for the $6M_{\odot}$, $Z = 0.02$ model shown in Figure 26. Time-dependent mixing is required to produce $^7$Li in a HBB

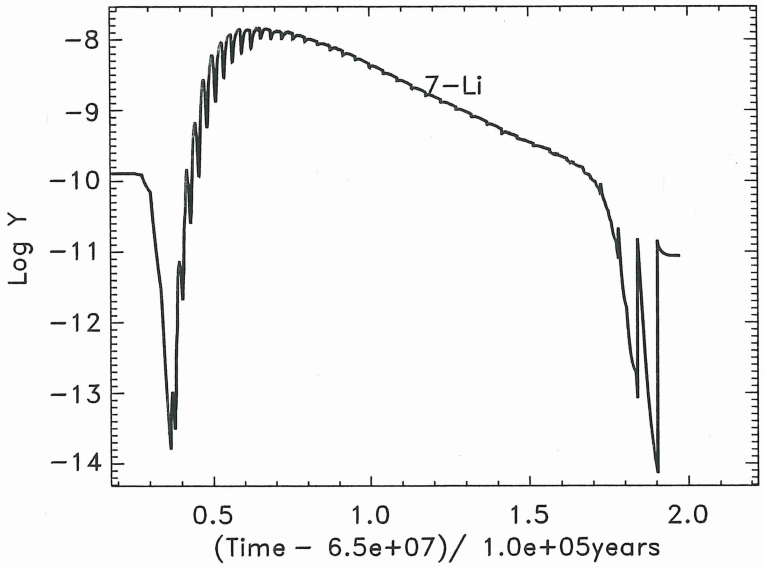


**Fig. 26.** The surface abundance of $^{7}$Li during the TP-AGB phase for a $6M_{\odot}$, $Z = 0.02$ model

calculation because the nuclear timescale for the reactions involved in the Cameron-Fowler mechanism are similar to the convective turnover timescale (see Fig. 2 in [149]).

It is still an open question whether or not AGB stars contribute to the production of $^{7}$Li in the Galaxy [150, 151]. There are many uncertainties involved in the production of $^{7}$Li in AGB models, including the mass-loss rates used and the treatment of convective mixing [152]. Mass-loss rates for AGB stars, such as the formula given by Vassiliadis & Wood [106] and Blöcker [107], have a superwind phase which occurs during the final few thermal pulses. The superwind phase results in a period of rapid mass loss, and most of the convective envelope is lost during this time. Thus the composition of the envelope at the start of the superwind phase critically determines the contribution AGB stars make to the enrichment of the interstellar medium. In Figure 26 most of the $^{7}$Li has been destroyed by the time the superwind phase starts.

### 5.8 HBB and the C, N, and O isotopes

Hot bottom burning first alters the envelope abundance of the CNO isotopes by the CN cycle and later, by the ON cycles. There is also a fourth cycle involving the destruction of $^{19}$F to produce $^{16}$O. The CN cycle burns $^{12}$C first into $^{13}$C and later into $^{14}$N, which reduces the $^{12}$C/$^{13}$C ratio from the pre-AGB value of $\approx 20$ to close to $4 - 5$, see Figure 27. The $^{14}$N abundance

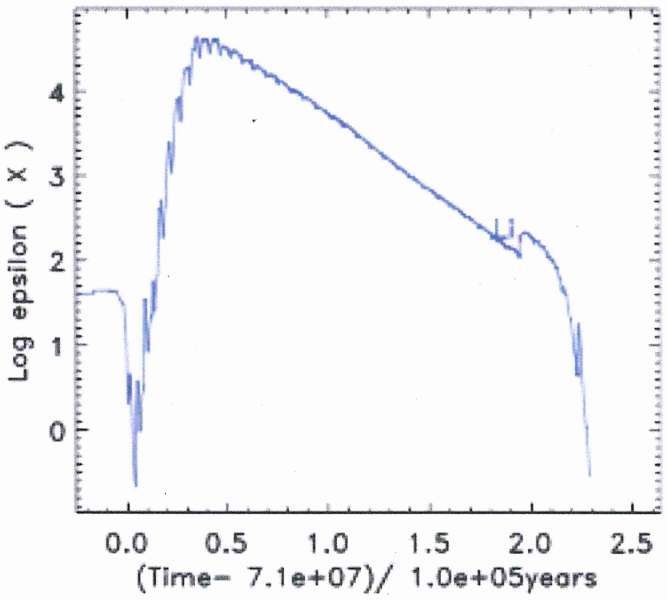


**Figure 27.** The surface abundance of $^{7}$Li during the TP-AGB phase for a $6\,M_{\odot}$, $Z = 0.02$ model. The units on the $y$-axis are $\log_{10}(n(Li)/n(H)+12)$ and time on the $x$-axis is scaled such that $t = 0$ is the beginning of the TP-AGB. The lithium-rich phase lasts for about 200 000 years.

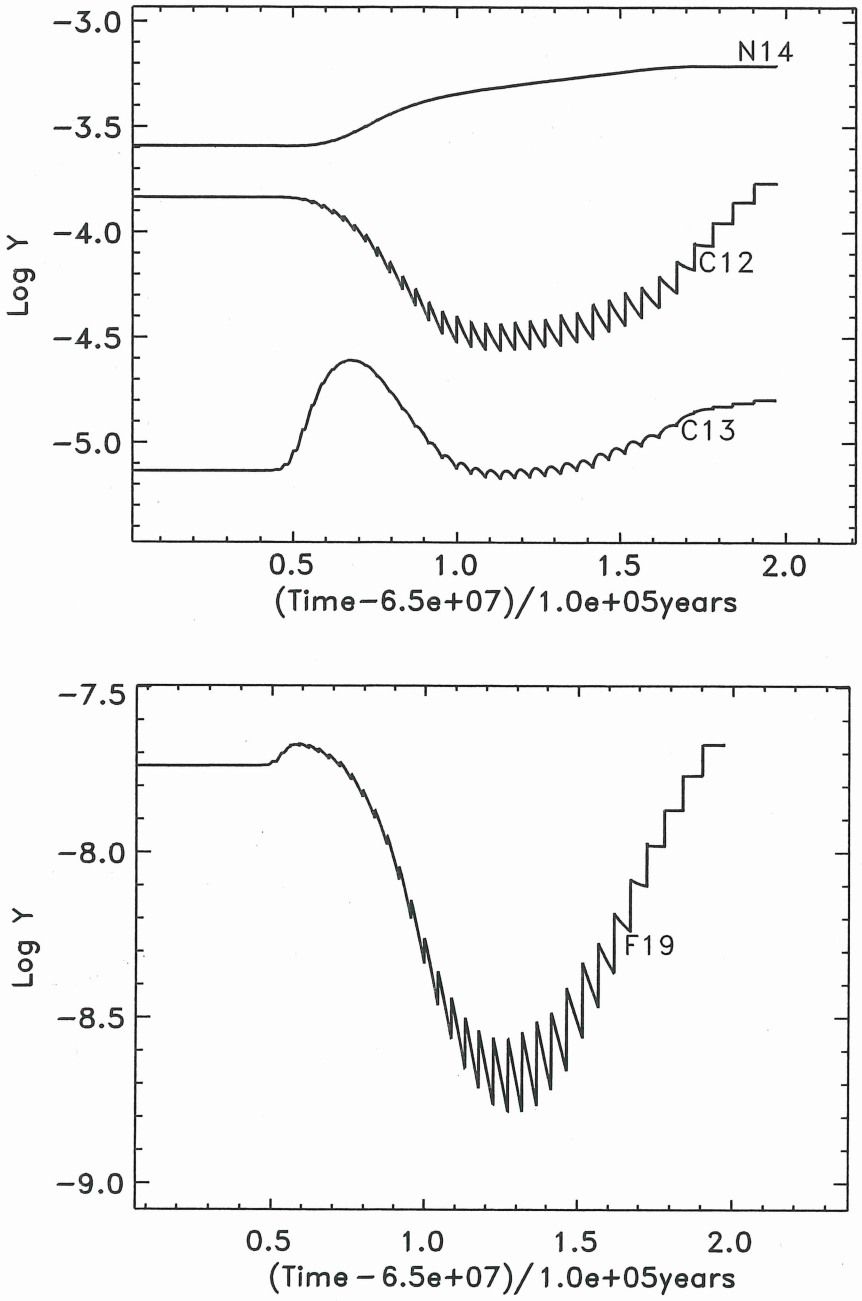


**Fig. 27.** The surface abundances evolution of C, N, and F during the TP-AGB phase for the $6M_{\odot}$, $Z = 0.02$ model. The final $^{12}C/^{13}C$ and C/O ratios are $\sim 10$ $\sim 0.4$, respectively

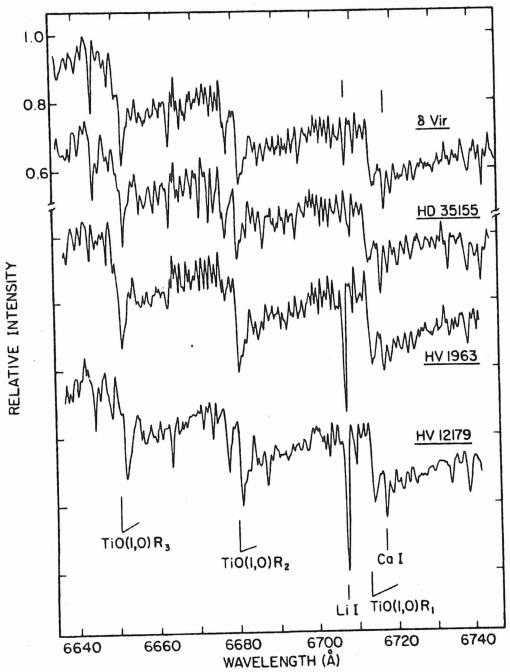


FIG. 1.—Sample spectra illustrating the Li I resonance doublet. An entire echelle order is shown: note the very strong Li I feature in the SMC stars (HV 1963 and HV 12179) as compared to the two Galactic red giants. Note also that this region is blanketed by TiO absorption.

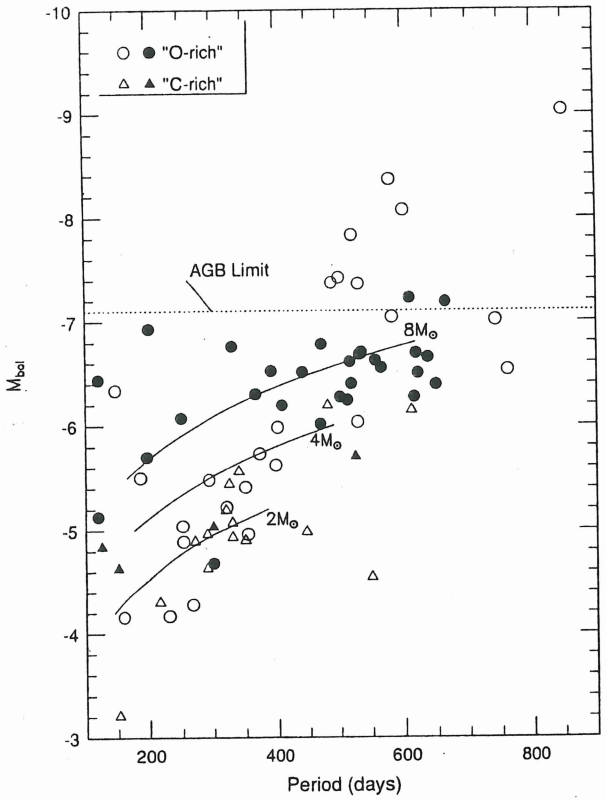


FIG. 6.—Combined $M_{bol}$-$P$ diagram for the Magellanic Clouds with the filled symbols denoting the Li-strong stars. The segregation of the Li-strong stars to the most luminous of the AGB stars is striking. Note that no AGB stars with detectable Li I are found at luminosities significantly exceeding the AGB limit. A few AGB stars with $M_{bol} > -6$ show detectable Li I lines. The solid curves denote evolutionary tracks for AGB stars taken from the equations given in Wood et al. (1983) for fundamental pulsators.

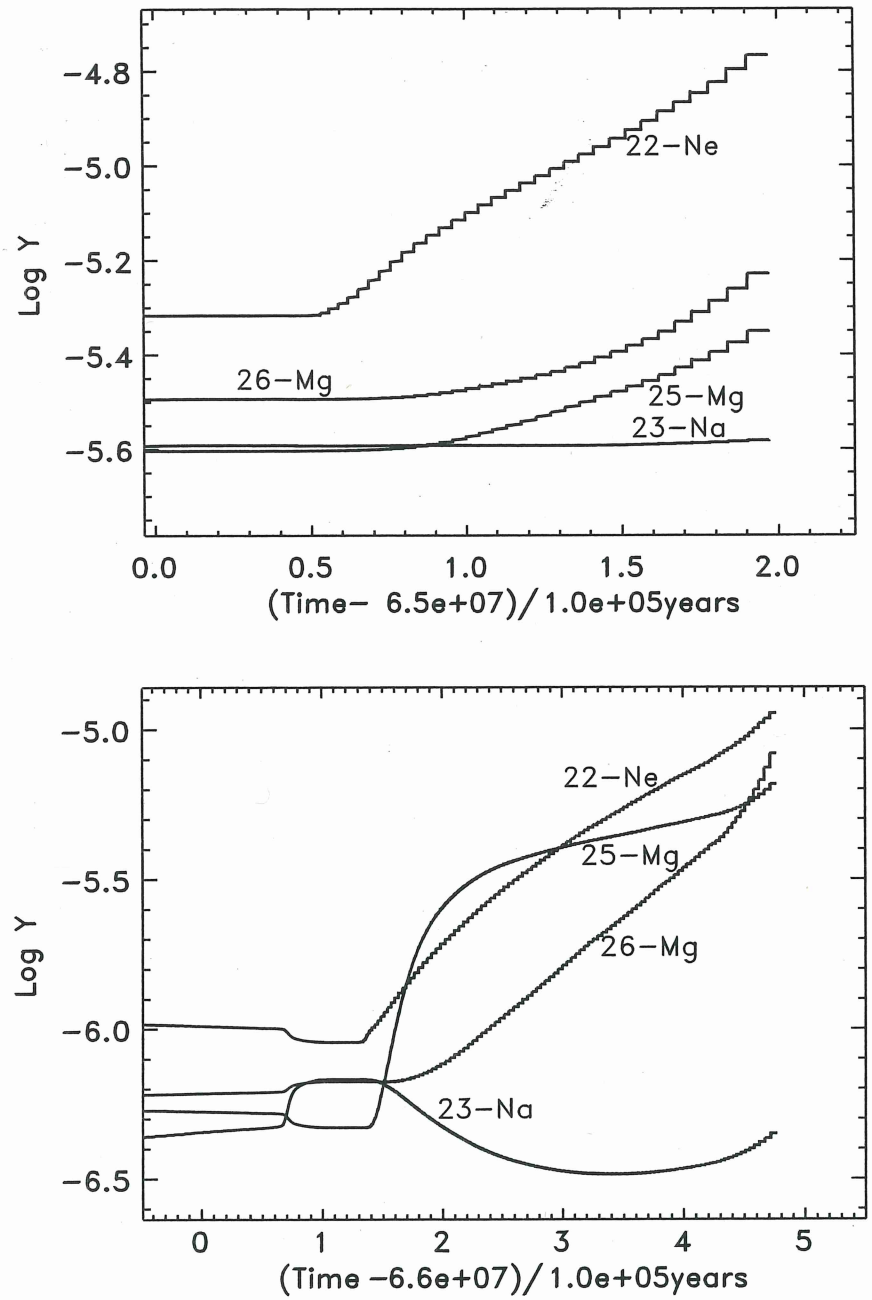


**Fig. 28.** The surface abundances evolution of $^{22}$Ne, $^{23}$Na, and the neutron-rich Mg isotopes during the TP-AGB for the $6M_{\odot}$, $Z = 0.02$ model (top panel), and for the $6M_{\odot}$, $Z = 0.004$ model (bottom panel)

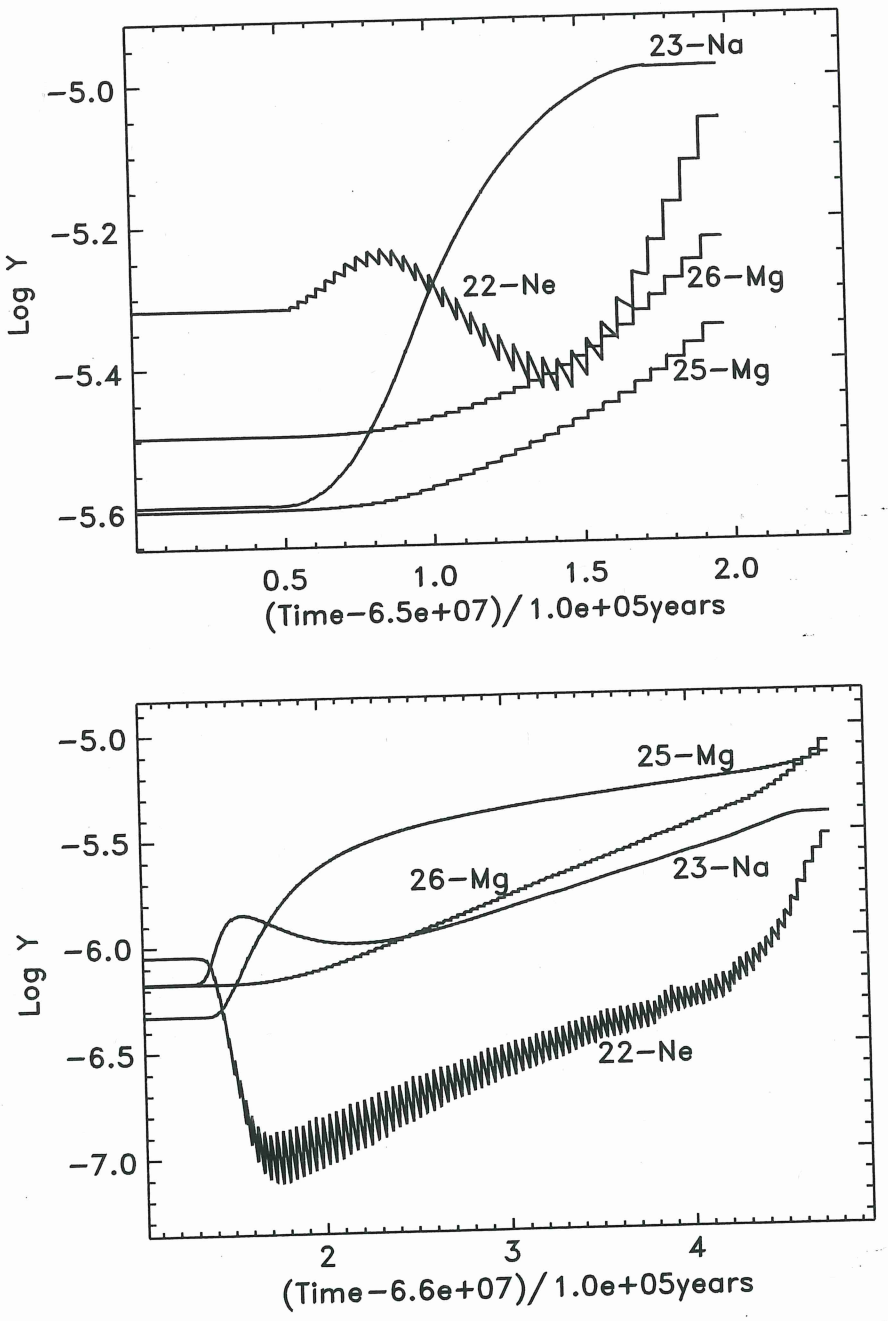


**Fig. 29.** Same as Figure 28, but using the NACRE rates for the Ne-Na and Mg-Al chains

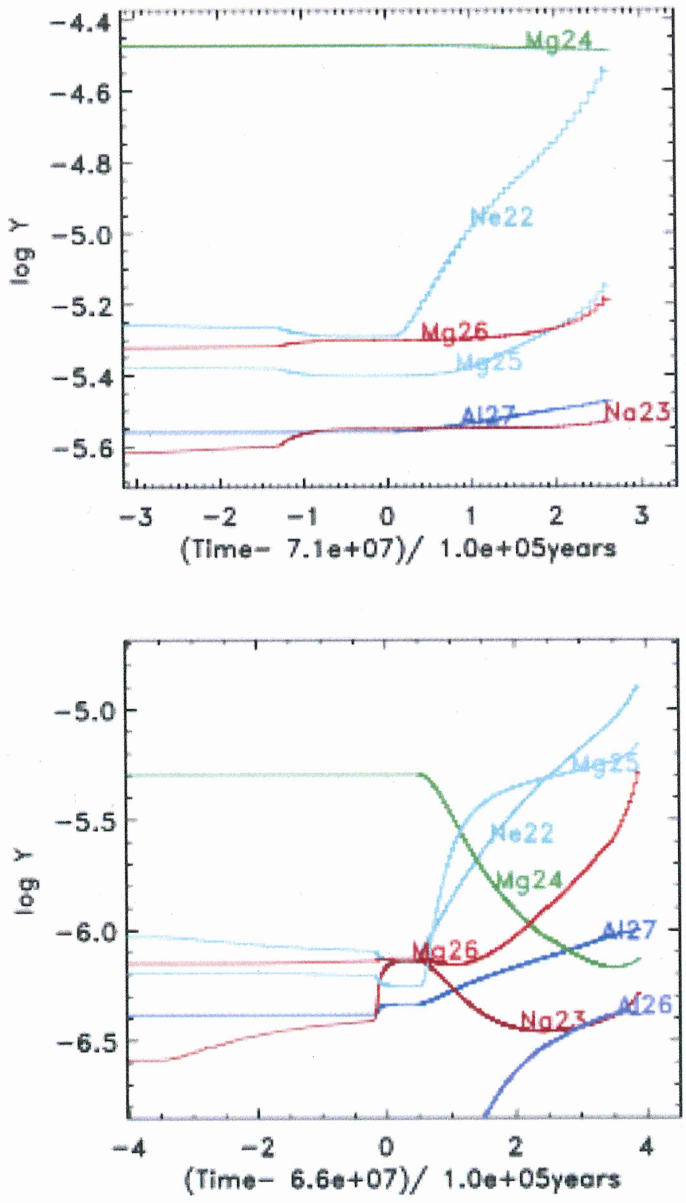


**Figure 25.** The evolution of various species involved in the Ne–Na and Mg–Al chains at the surface of the $6\,M_{\odot}$, $Z = 0.02$ model (upper panel) and $6\,M_{\odot}$, $Z = 0.004$ model (lower panel) during the TP-AGB. Time on the $x$-axis is scaled such that $t = 0$ is the time at the first thermal pulse. Abundances on the $y$-axis are in units of $\log_{10} Y$, where $Y = X/A$, where $X$ is mass fraction and $A$ is atomic mass. Both calculations used the same set of of reaction rates and scaled solar abundances. The $6\,M_{\odot}$, $Z = 0.004$ model has been described previously in Karakas (2010).